BAND GAP-VOLTAGE OFFSET AND ENERGY PRODUCTION IN NEXT-GENERATION MULTIJUNCTION SOLAR CELLS

R. R. King, D. Bhusari, A. Boca, D. Larrabee, X.-Q. Liu,
W. Hong, C. M. Fetzer, D. C. Law, and N. H. Karam

Spectrolab, Inc., 12500 Gladstone Ave., Sylmar, CA 91342 USA

ABSTRACT: The potential for new 4-, 5-, and 6-junction solar cell architectures to reach 50% efficiency is highly leveraging for the economics of concentrator photovoltaic (CPV) systems. The theoretical performance of such next-generation cells, and experimental results for 3- and 4-junction CPV cells, are examined here to evaluate their impact for real-world solar electricity generation. Semiconductor device physics equations are formulated in terms of the band gap-voltage offset $W_{oc} \equiv (E_g / q) - V_{oc}$, to give a clearer physical understanding and more general analysis of the multiple subcell band gaps in multijunction cells. Band gap-voltage offset is shown experimentally to be largely independent of band gap E_g for a wide range of metamorphic and lattice-matched semiconductors from 0.67 to 2.1 eV. Its theoretical E_g dependence is calculated from that of the radiative recombination coefficient, and at a more fundamental level using the Shockley-Queisser detailed balance model, bearing out experimental observations. Energy production of 4-, 5-, and 6-junction CPV cells, calculated for changing air mass and spectrum over the course of the day, is found to be significantly greater than for conventional 3-junction cells. The spectral sensitivity of these next-generation cell designs is fairly low, and is outweighed by their higher efficiency. Lattice-matched GaInP/GaInAs/Ge cells have reached an independently confirmed efficiency of 41.6%, the highest efficiency yet demonstrated for any type of solar cell. Light I-V measurements of this record 41.6% cell, of next-generation upright metamorphic 3-junction cells with 40% target production efficiency, and of experimental 4-junction CPV cells are presented.
Keywords: multijunction, high-efficiency, concentrator, III-V, energy production, band gap-voltage offset, radiative recombination, detailed balance

1 INTRODUCTION

Multijunction III-V photovoltaic cells for terrestrial concentrator systems are the highest efficiency solar cell technology yet demonstrated, with conversion efficiencies over 40% since 2006 [1-5]. Lattice-matched GaInP/GaInAs/Ge cells built at Spectrolab have reached an independently confirmed efficiency of 41.6% under the standard terrestrial direct spectrum at 364 suns (36.4 W/cm²) concentration, the highest efficiency achieved to date for any type of solar cell [5]. These high efficiencies are extremely leveraging for reducing the cost of solar electricity, since they reduce all area-related costs of a photovoltaic system – balance-of-system costs like encapsulation, support structures, concentrating optics and trackers, as well as the area and costs of the cells themselves – needed for a given power output.

As high as III-V multijunction efficiencies are presently, practical cell efficiencies of 50% and higher are possible with new solar cell architectures having theoretical efficiencies of 70% and above. The increase in efficiency from 40% to 50% is an extremely important range, corresponding to a tipping point at which concentrator PV becomes the most economic solar electricity option, and is competitive with conventional electricity generation in many geographic areas even without government subsidies. In this paper, we examine the energy production in next-generation 3- to 6-junction concentrator solar cells with the changing spectrum over the course of the day, and analyze today's state-of-the-art 3- and 4-junction cells, to evaluate the real potential of transformative cell architectures capable of 50% efficiency and above.

2 MULTIJUNCTION CELL MODELING

Fundamental physical principles dictate some of the directions necessary for reaching higher efficiencies than in today's solar cells. Incorporation of four and even more junctions is important to reduce carrier
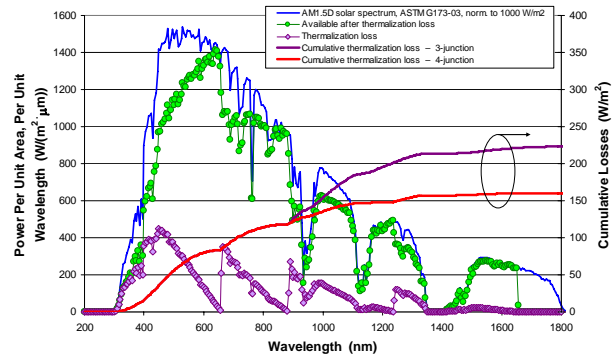
Fig. 1. Thermalization losses in an advanced 4-junction solar cell, and power available in the direct, terrestrial solar spectrum after thermalization losses as a function of wavelength. This 4-junction cell exhibits much lower cumulative loss from carrier thermalization to the band edges than in a typical 3-junction GaInP/GaInAs/Ge cell.

thermalization losses as electrons and holes excited far into their respective bands by high energy photons relax back to the band edges. Cells with 4 and more junctions have the additional significant benefit of lowering current density and I^2R series resistance power losses, especially important at the high current densities of concentrator cells. Efficient subcells with 2.0-eV band gaps and higher are needed to minimize thermalization loss in the top subcell. High quality subcells with band gaps in the 1.0-eV range must be incorporated in low cost multijunction designs, to avoid high thermalization loss in the Ge bottom cell of today's 3-junction cells, while subcells with low band gaps in the 0.7-eV range must continue to be used in order to capture as much energy as possible from the long wavelength portion of the solar spectrum. Finally, higher optical concentrations are favored as they narrow the distance between the quasi-Fermi levels of each carrier type and their respective band edges, allowing the cell voltage to come closer to that defined by the band gap.

Figure 1 plots the AM1.5 Direct ASTM G173-03 terrestrial solar spectrum [6], and the thermalization losses convoluted with the solar spectrum for a 4-junction concentrator solar cell with a 1.88/ 1.40/ 1.00/ 0.70 eV band gap combination, graphically showing the severity of this fundamental loss as a function of wavelength with respect to the subcell band edges, and the intensity available in different parts of the solar spectrum. The cumulative thermalization losses are plotted for the 4-junction design, and compared to a standard 3-junction GaInP/GaInAs/Ge cell, showing the substantially lower theoretical thermalization losses for the 4-junction cell.

Solar cells with four or more junctions also have significant technical challenges, which work against their theoretical efficiency advantages. One such challenge is that additional tunnel junctions are required to connect the added subcells in series, increasing the concern about parasitic light absorption in these interconnecting layers. Another important challenge, discussed in the energy production section of this paper, is that the finer division of the solar spectrum in cells with 4 or more junctions makes it more likely for a single subcell to limit the current of the entire multijunction cell stack, due to the effect of changing atmospheric conditions on the solar spectrum. Modeling of this effect indicates that the higher efficiency of 4- to 6-junction solar cell designs over the vast majority of operating times for CPV systems can more than compensate the current limitation at high air mass at the beginning and end of the day compared to conventional 3-junction cells.

2.1 Band Gap-Voltage Offset

In order to make useful efficiency predictions for next-generation multijunction solar cell designs, such as those described in [5] and elsewhere, a method is needed to deal easily and flexibly with semiconductors with a wide range of band gaps, covering the photon energies in the solar spectrum. A helpful way to think about the multiple semiconductors that form a multijunction cell is in terms of the band gap-voltage offset $W \equiv (E_g /q) - V$, particularly under open-circuit conditions $W_{oc} \equiv (E_g /q) - V_{oc}$ [1,5,7,8]. In the classic expression for non-equilibrium electron and hole concentrations, as in a solar cell base

$$pn = n_i^2 e^{qV/kT} \quad , \quad (1)$$

and the corresponding expression for the electron and hole quasi-Fermi level splitting, or voltage $V = \phi_p - \phi_n$ of the solar cell

$$V = \frac{kT}{q} \ln\left(\frac{pn}{n_i^2}\right) \quad , \quad (2)$$

information about the band gap E_g is contained in the intrinsic carrier concentration n_i, which varies exponentially with band gap, where

$$n_i^2 = N_C N_V e^{-E_g/kT} \quad . \quad (3)$$

This works well when dealing with single band gap solar cells with a well defined composition and value of n_i, such as in Si cells. When dealing with multijunction cells, with 3, 4, 5, 6, and up subcells, each with a

different band gap and different value of n_i, and many of which have some flexibility in the band gap in order to tune the multijunction cell for maximum efficiency, it becomes much less convenient to use this formulation with n_i and its very strong dependence on E_g.

A closer correspondence to the physics of the situation, in terms of the relationship of the electron and hole concentrations to the conduction band density of states N_C and the valence band density of states N_V, respectively, and a more convenient formulation as well can be found simply in the expression

$$pn = N_C N_V e^{-(E_g - qV)/kT} = N_C N_V e^{-qW/kT} \quad (4)$$

at the small expense of a little more writing. This simple shuffling of symbols gives a clearer representation of the dependence of electron concentration on the separation $(E_C - q\phi_n)$ of electron quasi-Fermi level from the conduction band energy, and similarly on the separation $(q\phi_p - E_V)$ for holes, since

$$qW = (E_C - q\phi_n) + (q\phi_p - E_V) =$$
$$(E_C - E_V) - q(\phi_n - \phi_p) = E_g - qV \quad . \quad (5)$$

The expression for the band gap-voltage offset $W \equiv (E_g /q) - V$ corresponding to Eq. (4) is then

$$W \equiv \left(\frac{E_g}{q}\right) - V = \frac{kT}{q} \ln\left(\frac{N_C N_V}{pn}\right) \quad . \quad (6)$$

It is often useful to consider the band gap-voltage offset $W_{oc} \equiv (E_g /q) - V_{oc}$ under open-circuit voltage conditions. For a solar cell with unity diode ideality factor, W_{oc} is related to the diode saturation current density J_o by

$$W_{oc} = \left(\frac{E_g}{q}\right) - V_{oc} = \left(\frac{E_g}{q}\right) - \frac{kT}{q} \ln\left(\frac{J_{ph}}{J_o}\right) \quad (7)$$

where J_{ph} is the photogenerated current density, and conversely

$$J_o = J_{ph} e^{-E_g/kT} e^{qW_{oc}/kT} = \frac{n_i^2}{N_C N_V} J_{ph} e^{qW_{oc}/kT} \quad . \quad (8)$$

The band gap-voltage offset W_{oc} for a solar cell at open circuit is far more invariant with respect to band gap than is n_i, allowing one to treat semiconductors with widely differing band gaps with the same methodology. It is basically a measure of how close electron and hole quasi-Fermi levels are to the conduction and valence band edges at open circuit, and these separations between quasi-Fermi level and band edge for each carrier type tend to vary only slightly with E_g. Similarly, although J_o varies exponentially among semiconductors of different band gaps, making it difficult to use J_o itself as a measure of the relative quality – *i.e.*, how closely the recombination rate approaches its ideal value with zero SRH recombination – of different semiconductors with different band gaps, we can write Eq. (8) as

$$K_o \equiv \frac{J_o}{n_i^2} = \frac{J_{ph}}{N_C N_V} e^{qW_{oc}/kT} \quad . \quad (9)$$

The quantity $K_o \equiv J_o / n_i^2$ has nearly all the dependence on band gap E_g taken out of it by dividing J_o by n_i^2. Thus, the parameter $K_o \equiv J_o / n_i^2$ can be used to compare the relative level of recombination in semiconductors of different band gaps, underscoring the generality and physical significance of the quantity J_o / n_i^2 compared to J_o itself.

A sense of the relative insensitivity of W_{oc} can be gained from the expression for the open-circuit voltage of a solar cell for which the only recombination mechanism is radiative recombination in the solar cell base. Assuming constant minority-electron concentration throughout the base with thickness w and p-type doping concentration N_A, in low-level injection ($n << p$):

$$V_{oc} = \frac{kT}{q} \ln\left(\frac{J_{ph}\, \tau\, N_A}{qwn_i^2} \right) = \frac{kT}{q} \ln\left(\frac{J_{ph}}{qwBn_i^2} \right) \quad (10)$$

where J_{ph} is the photogenerated current density, B is the radiative recombination coefficient, $\tau = 1/BN_A$ is the minority-carrier lifetime due to radiative recombination, and the other symbols have their usual meanings. The main dependence on the band gap E_g can be separated out using Eq. (3):

$$V_{oc} = \frac{E_g}{q} - W_{oc} = \frac{E_g}{q} - \frac{kT}{q} \ln\left(\frac{qwBN_CN_V}{J_{ph}} \right) \quad (11)$$

and

$$W_{oc} = \frac{kT}{q} \ln\left(\frac{qwBN_CN_V}{J_{ph}} \right) \quad (12)$$

B, N_C, and N_V depend somewhat on E_g, and w and J_{ph} depend somewhat on specific device design, but the central point is that since these parameters appear in the logarithmic second term of Eq. (11), the V_{oc} depends only weakly on the band gap dependence of these parameters, resulting in a nearly constant band gap-voltage offset $W_{oc} = (E_g/q) - V_{oc}$ across a wide range of band gaps. This is very useful for first-order predictions of new types of subcells in multijunction solar cell design. The difference between measured band gap-voltage offset W_{oc} for a solar cell, and the W_{oc} predicted when the fundamental mechanism of radiative recombination is dominant, allows one to determine an upper bound for the voltage under ideal conditions, as well as the part available for improvement by reducing the non-fundamental recombination due to Shockley-Read-Hall (SRH) recombination.

One way to visualize the approximate constancy of $(E_g/q) - V_{oc}$ for different semiconductors is that B varies only slowly with E_g, and therefore the pn product in steady state, at which the photogeneration rate per unit volume J_{ph}/qw equals the radiative recombination rate Bnp, is roughly similar for a given incident photon flux. Because the density of states in the conduction band is similar for many semiconductors, and the same is true for the valence band, similar p and n among different semiconductors in steady state translates to roughly the same energy difference between the conduction band edge and the electron quasi-Fermi level, and the same is true between the valence band edge and the hole quasi-

Fermi level. Since the cell voltage is the difference between electron and hole quasi-Fermi levels, and these quasi-Fermi levels have a fairly constant offset from their respective band edges, the cell voltage differs from the band gap voltage by a constant value, to first order.

This invariance of W_{oc} is borne out experimentally as well, as illustrated in Fig. 2 revised from [8], in which the measured open-circuit voltage and experimental value of band gap-voltage offset W_{oc} at one sun are shown for metamorphic and lattice-matched single-junction solar cells grown at Spectrolab, over a wide range of semiconductor band gaps. A variety of direct-gap III-V solar cells are plotted, with band gaps ranging from AlGaInP solar cells with 2.1-eV band gap, down to metamorphic 50%-In GaInAs cells with 0.79-eV band gap. The experimental V_{oc} values closely parallel the measured E_g over the broad band gap range covered by these single-junction solar cells, confirming the observation that V_{oc} and E_g are related approximately by an additive constant.
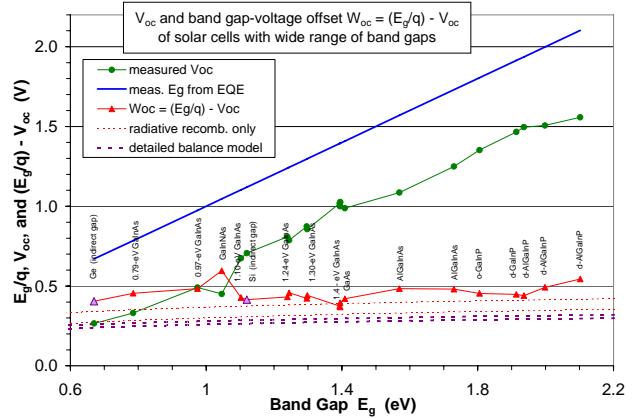
Fig. 2. Experimental V_{oc} for a wide range of single-junction solar cell band gaps, from 0.67 to 2.1 eV, showing that the band gap-voltage offset, $W_{oc} = (E_g/q) - V_{oc}$, is roughly constant over this range experimentally. The band gap-voltage offset W_{oc} is calculated for a semiconductor layer with radiative recombination only, and using the detailed balance model, also showing the approximate constancy of W_{oc} as predicted from theory. The measured band gap-voltage offset for some solar cell materials approaches the calculated value for radiative recombination only [8].

In addition to cells formed of direct gap semiconductors, a Ge single-junction solar cell with 0.67-eV indirect band gap grown at Spectrolab is also plotted for comparison in Fig. 2, with measured V_{oc} of 0.266 volts, and band gap-voltage offset W_{oc} of 0.404 V. Naturally, the radiative recombination coefficient is much lower in indirect-gap cells than in the other direct-gap III-V semiconductors, so different recombination mechanisms such as SRH recombination control W_{oc} for Ge cells. Silicon, with an indirect band gap of 1.12 eV, is the most widely-used solar cell semiconductor material. A record 25.0%-efficient silicon solar cell [9,10] has an open-circuit voltage V_{oc} of 0.706 V at one-sun, for a band gap-voltage offset of 0.414 V, and is also plotted in Fig. 2. It is interesting to note that experimental values of W_{oc} are still around 0.4 V for

high-performance Ge and Si solar cells, even though recombination mechanisms other than radiative recombination are controlling W_{oc} .

Although the band gap-voltage offset W_{oc} is relatively invariant with respect to E_g, it is instructive to calculate the trends in this dependence and typical values for the simple case in which radiative recombination is the sole recombination mechanism. This calculation is carried out in Appendix A, with approximate band gap dependences of the radiative recombination coefficient B and the conduction and valence band densities of states, N_C, and N_V, taken into account. These calculated values of W_{oc} for a semiconductor layer of thickness w in which only radiative recombination is present are plotted at one sun (0.100 W/cm^2) for comparison to the experimental values in Fig. 2. Upper and lower bounds of this calculated W_{oc} for radiative recombination only are shown, corresponding to $J_{sc} = 8$ mA/cm^2 and $w = 3.0$ μm for the upper bound, and $J_{sc} = 18$ mA/cm^2 and $w = 0.5$ μm for the lower bound, covering a typical range of these parameters for 3- to 6-junction solar cells at one sun. The difference $W_{oc} = (E_g/q) - V_{oc}$ calculated in this way for direct gap semiconductors with radiative recombination only, tends to decrease slightly with decreasing band gap, by only about 70 mV from ~0.41 to 0.34 V for the upper bound, and from ~0.35 to 0.28 V for the lower bound of W_{oc} in Fig. 2, as the band gap changes from 2.0 eV to 0.7 eV. At higher incident intensities the band gap-voltage offset W_{oc} will decrease, giving higher V_{oc} values. For instance at 1000 suns (100.0 W/cm^2), with 3 orders of magnitude higher J_{sc} than at one sun, W_{oc} can be expected to be about 180 mV = 3 × 60 mV lower than at one sun, ranging from ~0.17 to 0.10 V for the lower bound case over the same range of band gaps from 2.0 eV to 0.7 eV. Since the actual amount of photon recycling observed in a solar cell is dependent on the specific structure of the cell, photon recycling is not considered in this calculation, for simplicity, though it may be added to this analysis. It is informative to calculate the variation in W_{oc} with respect to E_g, using the approximations described in Appendix A. However, the central point is the approximate constancy of the band gap-voltage offset, allowing it to be a useful concept without being strongly affected by the band gap dependences of B, N_C, and N_V.

Comparing measured band gap-voltage offset $W_{oc} \equiv (E_g/q) - V_{oc}$ with that calculated from radiative recombination only is a helpful gauge of solar cell quality, especially when dealing with semiconductors of many different bandgaps, since it allows one to separate the fundamental radiative portion of carrier recombination, from the non-fundamental mechanism of SRH recombination that can in principle be eliminated by reducing the trap density to zero. At the 1.4-eV bandgap of 1%-In GaInAs, the experimental band gap-voltage offset of 0.369 V is very near to that calculated with radiative recombination only, indicating that nearly all of the recombination in this lattice-matched material is radiative, with very little SRH recombination. Metamorphic materials with higher lattice mismatch, such as 1.1-eV, 0.97-eV, and 0.79-eV GaInAs have offset voltages in the 430-490 mV range, still remarkably low in light of the 1.6%, 2.3%, and 3.5% lattice mismatches of these materials, respectively. It is interesting to note that the 0.428 V band gap-voltage offset of the 1.1-eV,

23%-In GaInAs subcell is nearly as low as that of the record efficiency silicon cell in Fig. 2 at the same band gap, in spite of the 1.6% lattice mismatch of this metamorphic GaInAs cell with respect to the Ge growth substrate.

Detailed balance limit calculations [11] generally give an even lower recombination rate than radiative recombination alone. The detailed balance model can be modified to calculate W_{oc} values as well, giving the lowest (most desirable) values of band gap-voltage offset allowable by the second law of thermodynamics. The band gap-voltage offset $W_{oc} = (E_g/q) - V_{oc}$ in the detailed balance limit is also plotted in Fig. 2, and details of the calculation are in Appendix B. An upper bound based on $J_{sc} = 8$ mA/cm^2, and a lower bound based on $J_{sc} = 18$ mA/cm^2 are calculated in the detailed balance case as well, using these current densities as typical values for multijunction subcells at one sun (0.100 W/cm^2). Again, the trend is toward decreasing W_{oc} as the band gap E_g decreases, dropping by about 50 mV from 0.31 to 0.26 V for the upper bound, and from 0.29 to 0.24 V for the lower bound of W_{oc} , as the band gap goes from 2.0 to 0.7 eV. Since the detailed balance arguments in [11] consider a grey-body thermal emission spectrum coming from the cell, without including the nearly monochromatic emission near the band gap energy usually associated with radiative recombination, one can interpret this to mean that all such near-band-gap emission is reabsorbed by electron-hole generation in the semiconductor before it is emitted, and thus the detailed balance model tacitly includes an assumption of ideal photon recycling [12]. This is consistent with the decrease in W_{oc} calculated with the detailed balance model, compared to the earlier calculation for radiative recombination only with no photon recycling, and underscores the fundamental nature of the detailed balance limit based only on thermodynamic arguments.

2.2 Energy Production

Energy production from photovoltaic power plants has been gaining increased attention from researchers for all types of solar modules, since it is the number of kilowatt-hours of electricity produced that has the most direct impact on the cost effectiveness of a solar electricity installation. It is a particularly salient topic for multijunction cells, since a shift in spectrum affecting current in one subcell not only reduces the output of that subcell, but limits the current of all other series-connected subcells as well, even though they may have ample photogeneration.

One of the most interesting questions in multijunction (MJ) photovoltaics is whether next-generation solar cell designs will be capable of increasing solar cell efficiencies from close to 42%, to over 50%, and whether those efficiency gains can be matched by corresponding increases in energy production. To increase the theoretical MJ cell efficiency beyond that of today's 3-junction cells, one must address the fundamental loss mechanism of thermalization of photoexcited charge carriers to their respective band edges. One of the most practical ways to do this is to divide the solar spectrum more finely into the narrower wavelength response ranges of the subcells in MJ solar cells with 4 and more junctions. Thus, although the gain from each additional subcell becomes smaller as one adds more subcells to the multijunction stack, the use of

4-, 5-, and 6-junction cells is difficult to avoid in the design of CPV cells with 45-50% efficiency and higher. In this light, the question of how energy production is affected by cell designs with 4 and more junctions is then more than a curiosity of device physics, but becomes highly relevant for the practicality of 50%-efficient CPV solar cells.

Energy production in multijunction solar cells has been the topic of a number of excellent articles. Detailed balance calculations for theoretically optimum band gap combinations in 1- to 6-junction cells, using solar spectra measured over one day were made in [13]. 3- to 6-junction cell energy production calculated for practical subcell band gap combinations drawn from actual semiconductor material systems, with radiative recombination, series resistance and grid shadowing, and other real-world efficiency losses included, was treated in [14]. Later papers have given detailed calculations of energy production in MJ cells, modeling its dependence on operating cell temperature and solar spectra under representative meteorological conditions at potential sites for CPV deployment [15-18], using actual solar irradiance measurements or the SMARTS model [19,20] based on measured solar spectra transmitted through the atmosphere.

The most fundamental atmospheric effect for PV energy production is that of increasing air mass on absorption of the solar spectrum, with increasing sun angle as a function of time of day and day in the year. The effects of air mass on spectrum must be contended with even on non-hazy days with the highest direct normal irradiance of solar insolation, the most significant days for CPV system energy production. As shown in Fig. 3 [14], the effect of air mass on the intensity of light transmitted through the atmosphere varies fairly gradually with respect to wavelength, but shorter wavelengths around the 400-700 nm range are attenuated more strongly than the longer wavelengths, causing the upper subcells in a multijunction stack, *e.g.*, the GaInP top subcell of a 3-junction cell, to limit the current density of the other subcells. Multijunction cells with more than 3 junctions tend to use higher band gap top subcells, increasing their sensitivity to the photon flux available at short wavelengths, which can lead to greater current limitation of cells with 4, 5, 6, and more junctions by the top subcell under non-standard spectra. The core question is how much can this current limitation at high air masses erode the potentially higher energy production of 4- to 6-junction cells compared to today's 3-junction cells?

Multijunction cell energy production over a typical year, taking into account cell operating temperature, and incident spectrum variations due to haze, aerosol optical depth, partial cloud cover, and other weather conditions at representative geographic locations, is important to be able to predict at each potential CPV deployment site, since this gives the final amount of energy that the CPV power plant will be able to produce and sell. A full calculation requires a complex set of spectral data and an assessment of how representative the spectra used for modeling are for the CPV site under consideration. In this paper, we consider a simple formulation of the problem, looking only at the dominant variation of the spectrum due to changing air mass, in order to gain insight into the core issue of current limitation by one
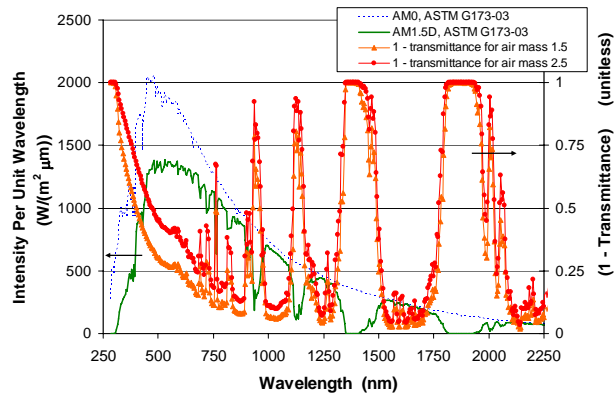
Fig. 3. Attenuation of light intensity due to the atmosphere, for air mass 1.5 and 2.5 [14].

subcell in a multijunction cell stack with changing spectrum in general. In this way, the treatment is focused on the extent to which efficiency gains at the design spectrum, from additional solar cell junctions, will also be available in the total energy produced, calculated in a general framework without the need for specific meteorological input, only the air mass based on sun angle geometry.

To calculate the effects of changing air mass and resulting changes in the solar spectrum on the energy production of 3-, 4-, 5-, and 6-junction solar cells, the band gap-voltage methodology above was used together with the standard current-voltage characteristic equation for each of the subcells with varying band gap, expressed as subcell voltage V as a function of current density J, where J is the same for all subcells in the series-interconnected multijunction stack at a given operating point. The subcell voltages are then summed to give the multijunction cell efficiency and energy production under the solar spectrum, calculated throughout the day on the autumnal equinox at 36° latitude as a function of air mass, by finding the absorption coefficient at each wavelength from comparison of the AM0 extraterrestrial solar spectrum and the standard ASTM G173-03 AM1.5 Direct spectrum for concentrator cells. The aerosol optical depth (AOD) for the standard ASTM G173-03 AM1.5 Direct standard spectrum is 0.084 at 500 nm. The autumnal equinox provides a reasonable midpoint representing the year as a whole, and thus was chosen as a typical day in the year with respect to positions of the sun and resulting air masses.

Since the emphasis is on practical solar cell designs, subcell band gap combinations for 4-, 5-, and 6-junction cells were chosen to be anchored by well-known subcell semiconductor materials such as (Al)GaInP, (Al)GaAs, and GaInAs, and with the other subcell band gaps demonstrated experimentally in lattice-matched, metamorphic, or wafer-bonded cell configurations, rather than by choosing the theoretical optimum band gaps. The bottom subcell was chosen to be 0.67 eV in each case so that the same portion of the solar spectrum contributes to photogeneration for each cell type, but the bottom subcell may be formed from semiconductors other than Ge, such as metamorphic GaInAs. The band gap combinations modeled are 1.88/ 1.40/ 0.67 eV for 3-junction, 1.88/ 1.44/ 1.04/ 0.67 eV for 4-junction, 1.95/ 1.70/ 1.40/ 1.12/ 0.67 eV for 5-junction, and 2.00/ 1.78/ 1.48/ 1.22/ 0.98/ 0.67 eV for 6-junction cells.

The solar concentration corresponds to 50.0 W/cm^2 (500 suns) at an air mass of 1.5. The modeling uses realistic values of band gap-voltage offset W_{oc} with precedent in mature semiconductor materials systems, rather than theoretical values, and specific cell resistances grounded in solar cell measurements. These realistic cell modeling parameters correspond to approximately 40% efficiency for the 3-junction cells over most of the day. The front metal grid spacing was optimized for each cell design, taking into account the different tradeoff between shadowing and resistance at the various current densities of the 3-, 4-, 5-, and 6-junction cells. The subcells above the bottommost subcell were current balanced under the spectrum at 9:00 AM on the autumnal equinox, which in this treatment is the same as at 3:00 PM. Earlier work [14] has shown that optimizing current balance among the subcells of the multijunction cell at this time results in more nearly optimal energy production over the day than optimizing at solar noon. The top subcells in the various multijunction cell designs are thinned to achieve some optical transparency for current matching, with higher optical transparency in the designs with a greater number of junctions. With the shifting spectrum and GaInP-like absorption coefficients, this top subcell transparency tends to become greater at high air mass for a constant cell thickness, and the relatively small impact that this effect has on energy production is included in the modeling.

The illuminated J-V characteristics of subcells in a 6-junction concentrator solar cell are shown in Fig. 4 together with the overall 6-junction cell characteristic, at 6.25 hours (6:15 AM) in Fig. 4a when the air mass is very high, and at the design point of 9.00 hours (9:00 AM) in Fig. 4b. The 2.00, 1.78, 1.48, 1.22, 0.98, and 0.67 eV subcell band gaps used in the 6-junction cell modeled here can be produced using metamorphic semiconductors, inverted growth, semiconductor bonding technology, and other methods, in one of several next-generation cell architectures described, for example, in [5]. As one can see, at the low sun angles and high air masses very early in the morning and late in the afternoon, there is a great deal of current mismatch among the subcells. However, for most of the day, and importantly, during the times that the greatest solar intensity is available, the subcell currents are much better matched, closer to the case at 9.00 hours. The progression of subcell current densities divided by incident intensity, i.e., the subcell responsivities in A/W are plotted throughout the day in Fig. 5.

The lower current densities for the top subcell (subcell 1) at high air mass result in a lower ratio between subcell 1 and subcell 2 photogenerated current densities, termed the J-ratio, in conventional 3-junction solar cells as well as for 6-junction solar cells, due to the greater attenuation of short wavelengths in the atmosphere with increasing air mass. This results in lower short circuit current density J_{sc} / intensity, and lower multijunction (MJ) cell efficiency for very high air masses, as shown in Fig. 6 for a 6-junction cell. However, the lower current densities are partially offset by higher MJ cell fill factor FF when the subcells are not current balanced. The opposing trends of FF and J_{sc} / intensity, as well as MJ cell efficiency, are plotted over the day in Fig. 7, (a) for 6-junction cells and (b) for 3-

(a)

(b)
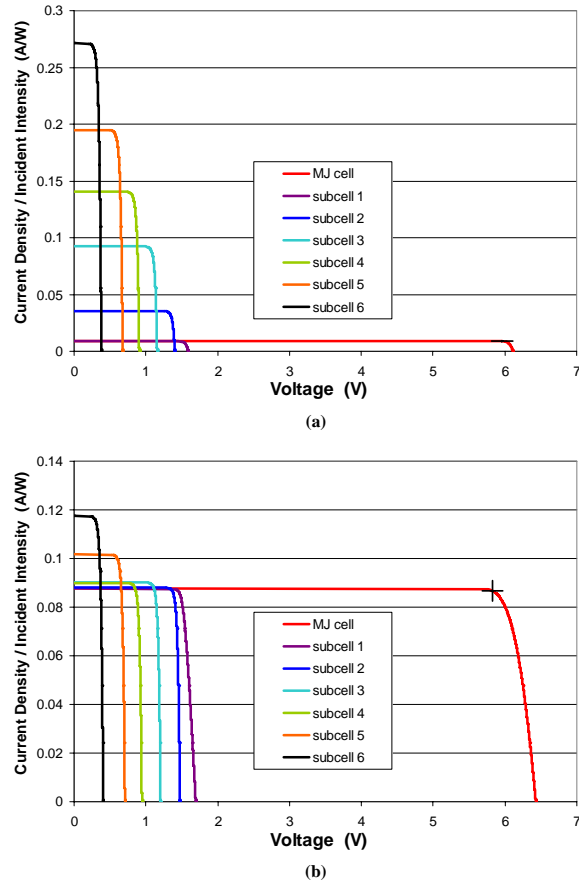
Fig. 4. Illuminated J-V characteristics of subcells in a 6-junction concentrator solar cell, together with the overall 6-junction cell characteristic, (a) at 6.25 hours (6:15 AM) with a very high air mass, and (b) at the design point of 9.00 hours (9:00 AM) on the autumnal equinox at 36° latitude.
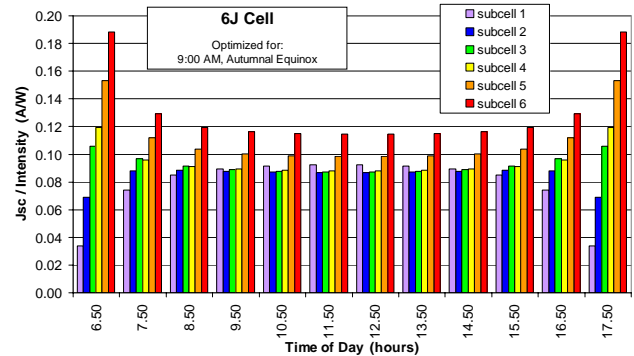
Fig. 5. Progression of subcell current densities divided by incident intensity, i.e., the subcell responsivities in A/W, for a 6-junction cell throughout the day.
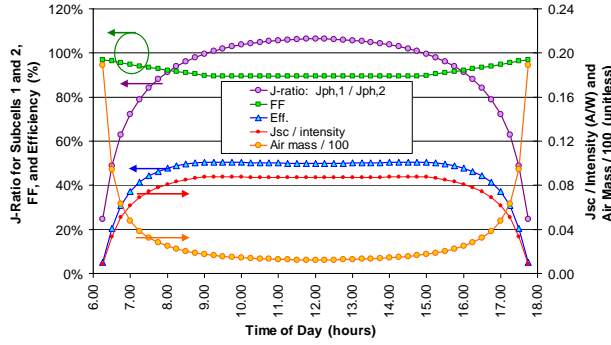
Fig. 6. J-ratio between subcells 1 and 2, multijunction cell efficiency, J_{sc} / intensity, and air mass plotted throughout the day on the autumnal equinox for a 6-junction solar cell.

(a)

(b)
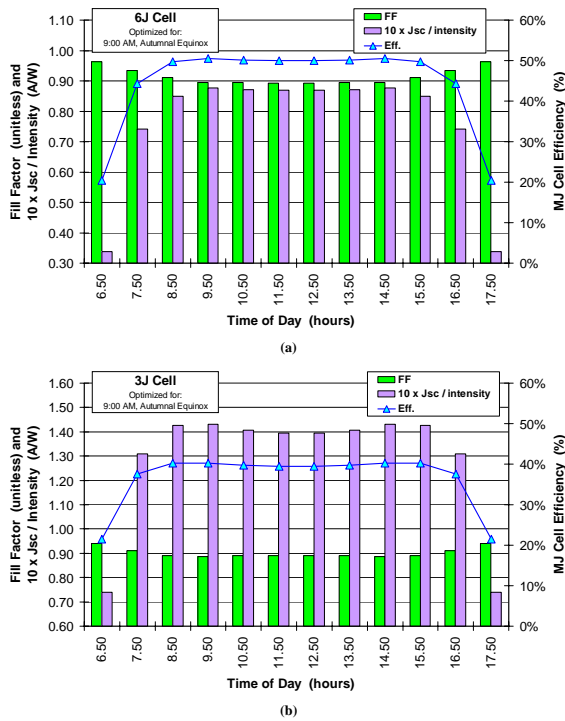
Fig. 7. The opposing trends of FF and J_{sc} / intensity plotted over the day for (a) 6-junction and (b) 3-junction cells, as well as the multijunction cell efficiency at each time.

Figure 8 plots the multijunction cell efficiency over the course of the day as calculated in this treatment, for 3-, 4-, 5-, and 6-junction cells. At 6.25 hours (6:15 AM), the 6-junction cell has the lowest efficiency, with higher efficiency for the 5J, 4J, and 3J cells. From 6.25 hours (6:15 AM) through 7.25 hours (7:15 AM), the 4-junction cell actually has higher efficiency than the other types of cells, including the conventional 3J cell, for the band gap combinations modeled here. By 7.50 hours (7:30 AM) the 6-junction cell efficiency exceeds that the 4J cell, and thereafter is the highest efficiency cell type, over the most significant energy-producing hours of the day. Thus the 6-junction cell has higher efficiency than devices with fewer subcells, not only at the design point

for which the upper subcells are current balanced, but also over a wide range of the relevant spectral conditions throughout the day at which the subcells are not perfectly current balanced. As a result, the 6-junction cell has higher energy production over this typical day than designs with fewer subcells, including conventional lattice-matched 3-junction cells, owing to the higher efficiency design, lower carrier thermalization losses, and lower series resistance losses of the 6-junction cell.
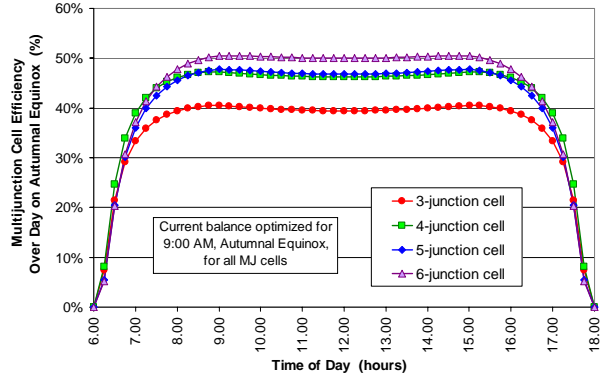
Fig. 8. Multijunction cell efficiency over the course of the day, modeled for 3-, 4-, 5-, and 6-junction cells on the autumnal equinox.

The modeled cumulative energy produced per unit area over the day is shown in Fig. 9, clearly showing that the higher efficiency 4- and 5-junction cell designs produce more energy than conventional 3-junction cells, and 6-junction cells produce more than any of the other cell designs by the end of the day. These trends are summarized in Table 1, showing the peak MJ cell efficiency (near the design point at 9:00 AM), the efficiency over the day, defined as

$$\text{efficiency over the day} = \frac{\text{cell output energy for the day}}{\text{light energy incident on the cell during the day}}$$

(13)

and the spectrum utilization factor, defined as

$$\text{spectrum utilization factor} = \frac{\text{efficiency over the day}}{\text{peak MJ cell efficiency}}$$

(14)

for 3-, 4-, 5-, and 6-junction cells. Peak efficiencies are 40.5% and 50.5% for 3-junction and 6-junction cells respectively, while the corresponding efficiencies over the day are 38.6% and 47.7%. Interestingly, the spectrum utilization factor is quite high, in the 0.94-0.96 range for 3- to 6-junction cells, with only a slight tendency for lower values in the 5J and 6J cells for the band gaps chosen here. The higher efficiencies of the 4J, 5J, and 6J cell designs far outweigh the effects of spectrum utilization on energy production in this study. This indicates that current limiting behavior in solar cells with 4 and more junctions due to changing spectrum may be less of a concern than originally feared, opening the door a bit wider to pursuing the high-efficiency potential of these advanced multijunction cell designs.

Fig. 9. Modeled cumulative energy produced per unit area over the day, clearly showing that the higher efficiency 4- and 5-junction cell designs produce more energy than conventional 3-junction cells, and 6-junction cells produce more than any of the other cell designs by the end of the day.

Table 1. Peak multijunction cell efficiency, the efficiency over the day, and spectrum utilization factor, as defined in the text, calculated for 3-, 4-, 5-, and 6-junction cells.

	3-junction	4-junction	5-junction	6-junction
Peak multijunction solar cell efficiency during day	40.5%	47.2%	47.7%	50.5%
Efficiency over day = Cell output energy during day / Energy in incident spectrum during day	38.6%	45.1%	45.1%	47.7%
Spectrum utilization factor over day = Efficiency over day / Peak multijunction solar cell efficiency	0.954	0.956	0.944	0.943

3 EXPERIMENTAL CELL PERFORMANCE

These advances in understanding are beginning to have an impact on experimental solar cell efficiencies. Upright metamorphic 3-junction GaInP/GaInAs/Ge concentrator cells, of the type that were first to reach over the 40% efficiency milestone, are now being inserted into manufacturing production as the C4MJ cell. A schematic cross section of this type of metamorphic cell is shown on the right side of Fig. 10, compared to a lattice-matched 3-junction cell on the left. As shown in Fig. 11, pilot production runs of the C4MJ terrestrial concentrator cell have demonstrated average efficiency of 39.4%, nearly an absolute efficiency point higher than the previous C3MJ cell generation, and are expected to reach 40% average efficiency in production.

Lattice-matched GaInP/GaInAs/Ge cells built at Spectrolab have reached an independently confirmed efficiency of 41.6% under the standard terrestrial direct spectrum at 364 suns (36.4 W/cm^2) concentration, the highest efficiency yet demonstrated for any type of solar cell [5]. The illuminated I-V characteristic of this record cell, as verified by the independent test lab at the National Renewable Energy Laboratory (NREL) for the standard ASTM G173-03, AM1.5 Direct spectrum at 25°C, is plotted in Fig. 12, with measured V_{oc} = 3.192 V, J_{sc} / intensity = 0.1468 A/W, FF = 0.8874 , and efficiency = 41.6 % at 364 suns.

Fig. 10. Schematics of the layer structures of lattice-matched and upright metamorphic 3-junction solar cells.

Fig. 11. Efficiency histograms of four generations of Spectrolab terrestrial concentrator cell products, from the C1MJ cell with 36.9% average production efficiency, C2MJ with 37.7%, C3MJ with 38.5%, and preliminary data for the next generation C4MJ cell, with 39.4% efficiency in early pilot runs. Average efficiency for the C4MJ cell is anticipated to reach 40%.

Fig. 12. Light I-V characteristic for a record 41.6%-efficiency concentrator solar cell, built at Spectrolab with a lattice-matched 3-junction cell structure, and independently verified at NREL [5].

The light I-V performance dependence on varying incident intensity for this record 41.6%-efficient cell is shown in Fig. 13. The efficiency, V_{oc}, and FF of this record cell are plotted at concentrations from 0.9 to 940 suns. The efficiency peaks at 41.6% at 364 suns and

drops for higher concentrations due to series resistance, but is still over 40% at 822 suns, and is 39.8% at 941 suns. The fill factor shows a broad plateau over ~2 decades in incident intensity, rising rapidly between 1 and ~4 suns due to increasing excess carrier concentration, and decreasing above ~400 suns due to series resistance.
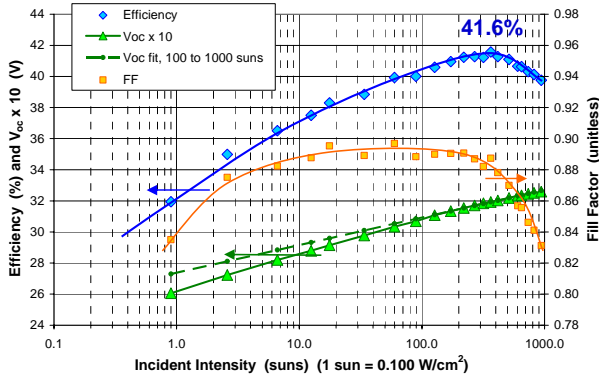
Fig. 13. Measured light I-V parameters of the 41.6%-efficient solar cell as a function of incident intensity. The cell is still over 40% efficient at 822 suns, and has 39.8% efficiency at 941 suns [5].

One may wonder about the extent to which a multijunction solar cell may be analyzed in a similar way as a single-junction cell to extract diode ideality factor from cell measurements, considering that it has multiple subcells connected in series that differ in band gap and diode saturation current density J_o, and may differ in diode ideality factor γ and photogenerated current density J_{ph}. The expression for the current-voltage characteristic of a multijunction solar cell is calculated in Appendix C, showing that in spite of these complications, the V_{oc} vs. J_{sc} characteristic for variable incident intensity for a multijunction solar cell can be used to accurately extract the sum of the subcell diode ideality factors.

Applying this treatment to the intensity dependence of V_{oc} for the record 41.6%-efficient cell in Fig. 13, this 3-junction cell has a total diode ideality factor of 4.03 in the intensity range from 1 to 10 suns (0.100 to 1.00 W/cm²), for an average of 1.34 per junction, and a V_{oc} increase at an average rate of ~80 mV per decade in incident intensity per junction. Separate measurements indicate that the Ge subcell diode ideality is close to unity, so that the average diode ideality factor γ for the upper GaInP and GaInAs subcells is actually closer to 1.51 in this intensity range. From 10 to 100 suns the total γ is 3.79, or an average of 1.26 per junction, corresponding to 75 mV per decade, per junction. In the concentration range from 100 to 1000 suns, the total γ is 3.08, or 1.03 average per subcell, for a rate of V_{oc} change per decade of 62 mV per junction. Thus over the 100 to 1000 sun range of interest, the average V_{oc} increase with concentration is fit fairly well by using diode ideality factor $\gamma = 1$ for each of the 3 subcells.

Measurements of the III-V subcells of 3-junction solar cells have shown decreasing diode ideality factor γ with increasing incident intensity, for both lattice-matched and metamorphic cell designs [21]. Since the measurements here and in [21] are V_{oc} vs. J_{sc}

measurements with varying incident intensity, rather than dark I-V measurements, analysis of the diode ideality factor is independent of the cell series resistance, greatly simplifying the measurement and improving accuracy of γ in the relevant high concentration range. Presumably the decrease in γ with increasing concentration is due to the presence of two recombination mechanisms in each subcell: one with diode ideality factor $\gamma = 1$ for radiative and Shockley-Read-Hall (SRH) recombination in the quasi-neutral regions of the cell base and emitter, where the concentration of one type of charge carrier is much larger than the other, and for which recombination current $J_{rec} = J_o \exp(qV / kT)$; and another mechanism with $\gamma \approx 2$ for SRH recombination in the space charge region between base and emitter and at unpassivated surfaces around the cell perimeter, where electron and hole concentrations are more similar, and for which $J_{rec} = J_o \exp(qV / 2kT)$. At higher incident intensities and higher cell voltage V, the $\gamma = 1$ mechanism dominates recombination current, bringing the overall diode ideality close to unity in each subcell. Potentially, as minority-carrier injection levels increase at high intensities, and electron and hole concentrations become closer to each other throughout the bulk of the cell, Auger recombination with characteristic diode ideality factor of $\gamma = 2/3$ can play a role to bring down the overall ideality factor.

Measured external quantum efficiency for each of the subcells in an experimental 4-junction lattice-matched AlGaInP/ AlGaInAs/ GaInAs/ Ge terrestrial concentrator solar cell is plotted in Fig. 14. In Fig. 15, the illuminated I-V curve of a prototype 4-junction terrestrial concentrator cell is plotted, showing its high-voltage, low-current characteristics which lead to lower resistive power loss compared with 3-junction cells [5]. These early prototype 4-junction concentrator cells have reached up to 36.9% efficiency at 500 suns (50 W/cm²) at Spectrolab in unconfirmed measurements. The independently confirmed light I-V curves of the earlier record 40.7%-efficient metamorphic 3-junction cell [1], the present record 41.6%-efficient lattice-matched 3-junction cell at 364 suns [5], and the same cell measured to have 40.1% efficiency at 822 suns, are also plotted for comparison.
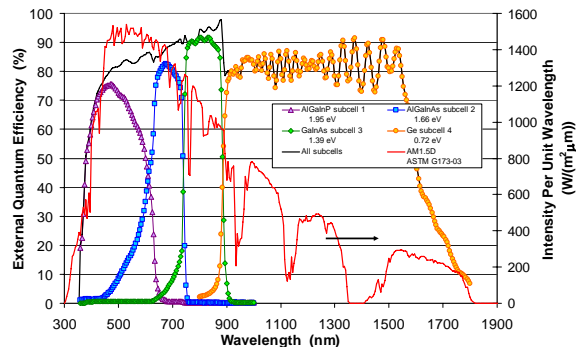
Fig. 14. Measured external quantum efficiency for the individual subcells of a 4-junction lattice-matched AlGaInP/ AlGaInAs/ GaInAs/ Ge terrestrial concentrator solar cell. The intensity per unit wavelength of the standard AM1.5D, ASTM G173-03 spectrum is plotted, to show available power in the response ranges of each subcell.
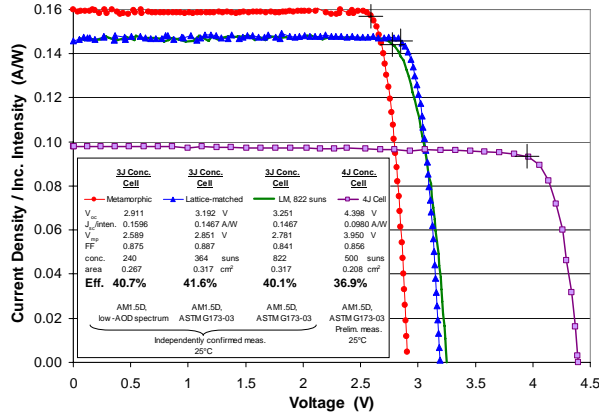
Fig. 15. Light I-V measurements for a 4-junction terrestrial concentrator cell with V_{oc} of 4.398 V, and preliminary efficiency of 36.9% at 500 suns. An earlier record 40.7% MM 3J cell [1], the present record 41.6% LM 3J cell at 364 suns, and the same cell with 40.1% measured efficiency at 822 suns, are plotted for comparison [5].

4   SUMMARY

By analyzing the potential performance of next-generation multijunction solar cells, both in terms of their efficiency under standard conditions and their energy production under a changing spectrum, the discussion in this paper aims to form a bridge between present and future high-efficiency solar cell designs and real-world solar electricity generation. The advantages of formulating semiconductor device physics equations in terms of the band gap-voltage offset $W_{oc} = (E_g/q) - V_{oc}$ are outlined, to facilitate analysis of solar cells with multiple band gaps in multijunction devices, and to build greater physical insight into the workings of photovoltaic cells. The band gap-voltage offset is shown experimentally to be nearly independent of semiconductor band gap E_g for a wide range of solar cell band gaps from 0.67 to 2.1 eV. The theoretical dependence of band gap-voltage offset on E_g is calculated from both the expected band gap dependence of the radiative recombination coefficient, and at a more fundamental level using the Shockley-Queisser detailed balance model, bearing out the weak band gap dependence observed experimentally.

Identifying which design features are important for energy production, and those that are of less concern, allows one to make informed decisions on research directions for advanced cell architectures that maximize efficiency and energy production. In particular, energy production in 4-, 5-, and 6-junction cells is found to be significantly greater than for the 3-junction cells considered here, since the higher efficiencies of these next-generation cell designs far outweigh the effects that the greater number of junctions has on spectrum utilization. Only the geometrical effects of changing air mass over the course of the day that are encountered at all photovoltaic installations were considered here, rather than site-specific atmospheric conditions, to keep the results as general as possible. Thus the spectral sensitivity of solar cells with 4-, 5-, and 6-junctions under the changing terrestrial solar spectrum may not be

as large a barrier to implementing these high-efficiency designs as thought initially.

Three-junction terrestrial concentrator solar cells are still expanding the limits of their full potential. The efficiency distribution for a pilot build of the C4MJ terrestrial concentrator cell product, with an upright metamorphic 3-junction structure and 40% target efficiency in manufacturing, is presented. The measured parameters of a 41.6%-efficient 3-junction cell [5], with the highest efficiency demonstrated to date for any type of solar cell, and of experimental 4-junction terrestrial concentrator solar cells are analyzed. The next generations of multijunction concentrator cells, capable of 45% or even 50% efficiency and correspondingly high levels of energy production, have the ability to transform the economics of solar electricity generation.

Appendix A: Band gap-voltage offset W_{oc} calculated for radiative recombination only in semiconductor layer

As discussed in the main text, although the band gap-voltage offset W_{oc} is relatively invariant with respect to E_g, it is helpful to calculate the trends in this dependence and typical values for the case in which the fundamental mechanism of radiative recombination is the only charge carrier recombination path. The radiative recombination coefficient B and conduction and valence band densities of states N_C and N_V vary among specific semiconductors, but the electron effective mass has a tendency to be lower for semiconductors with lower E_g [22]. An approximate linear relationship for electron effective mass m_e and band gap E_g can be fitted through a number of semiconductors, such that

$$m_e \approx bE_g \qquad (A1)$$

where b is a constant. Since N_C depends on $m_e^{3/2}$, this gives a rough proportionality of $N_C \propto E_g^{3/2}$, where we are considering primarily direct gap semiconductors. B can clearly vary by orders of magnitude between direct and indirect gap transitions. For direct gap semiconductors, which are of strong interest for III-V multijunction cells, Hall [23] gives an expression for B in terms of the band gap E_g and the effective mass m_e, based on equivalence of the radiative recombination rate in equilibrium and blackbody radiation absorbed via band-to-band processes as described by van Roosbroeck and Shockley [24], and the absorption coefficient in direct gap semiconductors described by Bardeen *et al.* [25]:

$$B = \frac{(2\pi)^{3/2}}{3} \frac{\hbar q^2}{m^2 c^2} \mu \left(\frac{m}{m_e + m_h} \right)^{3/2} \times$$

$$\left(1 + \frac{m}{m_e} + \frac{m}{m_h} \right) \frac{E_g^2}{(kT)^{3/2} (mc^2)^{1/2}} \quad . \quad (A2)$$

where m is the electron mass, m_h is the hole effective mass, c is the speed of light, and the equation is in CGS units. The dependence of the refractive index μ on E_g is considered to be relatively small here, and m_e is typically much smaller than m_h for many III-V semiconductors of interest. Including the dependence of m_e on E_g discussed above results in an approximate quadratic dependence of B on E_g

$$B = (f + gE_g)E_g \qquad (A3)$$

where f and g are constants. N_V is relatively similar for a variety of direct gap semiconductors, and for the purposes of this calculation is considered to be constant with respect to E_g. Taking into account these approximate trends of B, N_C, and N_V with respect to band gap E_g, fitting these parameters through their experimental values for GaAs at 1.424 eV, and for approximately constant values of J_{ph} and w as may be found in the subcells of a multijunction cell, the value of W_{oc} for which only the fundamental mechanism of radiative recombination is present can be calculated. As described in the text, photon recycling is not included in the above treatment, to obtain a conservative calculation of W_{oc}, and because it is dependent on the specific configuration of the solar cell, but it can be added to the analysis. The trend of this calculated W_{oc} with respect to E_g with only radiative recombination is plotted for comparison to the experimental values in Fig. 2, as discussed in the main text.

Appendix B: Band gap-voltage offset W_{oc} calculation from detailed balance model

It is interesting to calculate the limiting value of the band gap-voltage offset $W_{oc} = (E_g/q) - V_{oc}$ of a solar cell using the detailed balance model, since the minimum value of W_{oc} indicates the highest voltage a solar cell of a given band gap can achieve consistent with the second law of thermodynamics, for a given photogenerated current density. Knowing this detailed balance limit of W_{oc} then allows the solar cell designer to ask what mechanisms are responsible for the difference between experimental W_{oc} values and the fundamental limit, such as SRH recombination, low incident intensity, or incomplete photon recycling, and then address those non-fundamental losses to bring cell efficiency as close to the value allowed by physics as possible.

In their classic paper on "Detailed Balance Limit of Efficiency of p-n Junction Solar Cells," Shockley and Queisser calculate the highest efficiency of a single-junction solar cell that is consistent with thermodynamic first principles, based on the exchange of thermal radiation between a solar cell at temperature T_c and a blackbody radiator surrounding the cell at the same temperature, with which the solar cell is in equilibrium [11]. The basics of that argument are summarized here,

in order to calculate W_{oc} as a function of band gap in the detailed balance limit, as shown in Fig. 2.

The rate of carrier recombination in a semiconductor due to radiative recombination, $F_{c,rad}$, is proportional to the product of electron and hole concentrations, n and p, at a given quasi-Fermi level splitting qV in the semiconductor, such that

$$F_{c,rad}(V) = C_{rad} p n \qquad (B1)$$

where C_{rad} is the proportionality constant. The splitting between electron and hole quasi-Fermi levels qV determines the voltage V of the solar cell. $F_{c,rad}$ has units of s^{-1}, and the subscript c designates the solar cell as in [11]. To determine this proportionality constant, Shockley and Queisser considered a spherical solar cell in equilibrium with a blackbody radiator surrounding it, at the same temperature T_c as the solar cell. The rate F_{c0} of electron and hole generation due to the thermal radiation from the spherical blackbody radiator that enters the solar cell is

$$F_{c0} = At_c Q_c \qquad (B2)$$

where A is the solar cell area, t_c is the fraction of light incident on the cell that is transmitted through its outer surface into the semiconductor, and Q_c is the number of photons incident on the solar cell, per unit cell area, per unit time, with energy E greater than the band gap E_g of the semiconductor, for blackbody temperature T_c. Q_c has units of $cm^{-2}s^{-1}$. Since the cell and radiator are in equilibrium with each other, the rate at which carriers are recombining in the semiconductor through radiative recombination, and emitting photons back to the blackbody radiator, must be equal to the rate at which radiation from the blackbody radiator causes carrier generation in the solar cell, and

$$F_{c0} = At_c Q_c = C_{rad} n_i^2 \qquad (B3)$$

since for a semiconductor in equilibrium, $pn = n_i^2$, where n_i is the intrinsic carrier concentration in the semiconductor. Thus

$$C_{rad} = \frac{At_c Q_c}{n_i^2} \qquad . \qquad (B4)$$

When sunlight, or light from a blackbody radiator with $T > T_c$, is incident on the solar cell, the quasi-Fermi levels are separated by an energy qV, and the recombination current density J_{rec} is

$$J_{rec} = \frac{q F_{c,rad}(V)}{A} = \left(\frac{q t_c Q_c}{n_i^2} \right) p n \qquad (B5)$$

and using the general relation

$$pn = n_i^2 e^{qV/kT} \qquad (B6)$$

we have

$$J_{rec} = q t_c Q_c e^{qV/kT_c} = J_o e^{qV/kT_c} \qquad (B7)$$

and

$$J_o = qt_cQ_c \qquad . \qquad \text{(B8)}$$

The photon flux Q_c incident on the solar cell from the blackbody radiator at the same temperature T_c as the cell, with photon energy $E > E_g$, can be found from the Planck distribution of photon frequency ν from a blackbody [11]

$$Q_c = \frac{2\pi}{h^3 c^2} \int_{E_g}^{\infty} \frac{E^2}{e^{E/kT_c} - 1} dE = \frac{2\pi(kT_c)^3}{h^3 c^2} \int_{x_g}^{\infty} \frac{x^2}{e^x - 1} dx$$

(B9)

expressed here in terms of photon energy $E = h\nu$, where h is the Planck constant, and c is the speed of light, and simplified with a change of variable $x \equiv E/kT_c$. This definite integral can be approximated by observing that E_g of the solar cell is much greater than the thermal energy kT_c , and therefore $x >> 1$ over the range of integration, so that the integral can be approximated as

$$\int_{x_g}^{\infty} \frac{x^2}{e^x - 1} dx \approx \int_{x_g}^{\infty} \frac{x^2}{e^x} dx = \left[-\left((x+1)^2 + 1\right)e^{-x}\right]_{x_g}^{\infty}$$

(B10)

Again, since x is much greater than unity, $(x+1)^2 >> 1$, and

$$\int_{x_g}^{\infty} \frac{x^2}{e^x - 1} dx \approx \left[-(x+1)^2 e^{-x}\right]_{x_g}^{\infty} = (x_g + 1)^2 e^{-x_g}$$

(B11)

so that

$$Q_c = \frac{2\pi}{h^3 c^2} \int_{E_g}^{\infty} \frac{E^2}{e^{E/kT_c} - 1} dE \approx \frac{2\pi(kT_c)^3}{h^3 c^2}(x_g + 1)^2 e^{-x_g} = $$
$$\frac{2\pi(kT_c)^3}{h^3 c^2}\left(\frac{E_g}{kT_c} + 1\right)^2 e^{-E_g/kT_c}$$

(B12)

and for the ideal case of zero solar cell reflectance, $t_c = 1$, and

$$J_o = qQ_c = \frac{2\pi q(kT_c)^3}{h^3 c^2}\left(\frac{E_g}{kT_c} + 1\right)^2 e^{-E_g/kT_c}$$

(B13)

consistent with Refs. [11] and [26].

The band gap-voltage offset $W_{oc} = (E_g/q) - V_{oc}$ can be expressed in the detailed balance model by using this expression for J_o in Eq. (7)

$$W_{oc} = \left(\frac{E_g}{q}\right) + \frac{kT}{q}\ln\left(\frac{J_o}{J_{ph}}\right) = $$
$$\left(\frac{E_g}{q}\right) + \frac{kT}{q}\ln\left(\frac{2\pi q(kT)^3}{h^3 c^2}\left(\frac{E_g}{kT} + 1\right)^2 \frac{1}{J_{ph}}\right) + \frac{kT}{q}\ln\left(e^{-E_g/kT}\right)$$

(B14)

$$W_{oc} = \frac{kT}{q}\ln\left(\frac{2\pi q(kT)^3}{h^3 c^2}\left(\frac{E_g}{kT} + 1\right)^2 \frac{1}{J_{ph}}\right)$$

(B15)

The exponential dependence on E_g in the equation for J_o is taken out by expressing recombination in the cell in terms of W_{oc} above. The small dependence on E_g remaining is the natural log of terms that are quadratic in E_g . The value of W_{oc} in the detailed balance limit over a wide range of band gaps is plotted in Fig. 2. As described in the text, the detailed balance model essentially includes the phenomenon of photon recycling [12], and assumes that it is as effective as possible, consistent with the second law of thermodynamics.

Appendix C: Diode ideality factor extraction from multijunction cell I-V characteristics

In order to check the validity of parameter extraction from the current-voltage (I-V) curve of a multijunction solar cell, compared to the single-junction cell case, we can calculate the expression for the I-V characteristic of a multijunction solar cell as follows, neglecting series resistance and shunt conductance for simplicity.

Each subcell i in the multijunction solar cell is assumed to be described by the diode equation for a single junction:

$$J_i = J_{ph,i} - J_{o,i}\left(e^{qV_i/\gamma_i kT} - 1\right) \qquad \text{(C1)}$$

For positive solar cell operating voltages, unity is negligible compared to the exponential term in the equation, and we have:

$$J_i = J_{ph,i} - J_{o,i}e^{qV_i/\gamma_i kT}$$

and

$$V_i = \frac{\gamma_i kT}{q}\ln\left(\frac{J_{ph,i} - J_i}{J_{o,i}}\right) \qquad \text{(C2)}$$

For a concentration ratio X of light incident on the multijunction cell:

$$J_{ph,i} = J_{ph,i,1sun}X$$

and

$$V_i = \frac{\gamma_i kT}{q}\ln\left(\frac{J_{ph,i,1sun}X - J_i}{J_{o,i}}\right) \qquad \text{(C3)}$$

For a 3-junction cell, the current density J_{3J} is the same as in each of the subcells:

$$J_{3J} = J_1 = J_2 = J_3 \qquad \text{(C4)}$$

and the 3-junction cell voltage V_{3J} is the sum of the subcell voltages:

$$V_{3J} = V_1 + V_2 + V_3 = \frac{kT}{q}\sum_{i=1}^{3}\gamma_i\ln\left(\frac{J_{ph,i,1sun}X - J_i}{J_{o,i}}\right)$$

(C5)

This expression does not have the same form in general as the current density-voltage (J-V) characteristic of a single-junction solar cell, complicating extraction of

diode ideality factors from multijunction cell current-voltage data at a single light intensity.

However, when comparing open-circuit voltages of a multijunction cell with varying incident intensity, it is a different story, and at open circuit the sum of subcell diode ideality factors can be obtained in a similar way as for a single-junction cell. At open-circuit conditions, $J_i = 0$, and

$$V_{oc,3J} = \frac{kT}{q} \sum_{i=1}^{3} \gamma_i \ln\left(\frac{J_{ph,i,1sun} X}{J_{o,i}} \right) =$$

$$\frac{kT}{q} \sum_{i=1}^{3} \gamma_i \ln\left(\frac{J_{ph,i,1sun}}{J_{o,i}} \right) + \frac{kT}{q} \sum_{i=1}^{3} \gamma_i \ln X \qquad \text{(C6)}$$

so that the dependence of the open-circuit voltage of a 3-junction cell on concentration C is simply:

$$V_{oc,3J} = V_{oc,3J,1sun} + (\gamma_1 + \gamma_2 + \gamma_3)\frac{kT}{q} \ln X =$$

$$V_{oc,3J,1sun} + (\gamma_1 + \gamma_2 + \gamma_3)\frac{kT}{q} \frac{1}{\log_{10} e} \log_{10} X$$

(C7)

Thus the dependence of $V_{oc,3J}$ for a 3-junction cell on X has the same form as for a single-junction cell:

$$V_{oc,1J} = \gamma \frac{kT}{q} \ln\left(\frac{J_{ph,1sun}}{J_o} \right) + \gamma \frac{kT}{q} \ln X =$$

$$V_{oc,1J,1sun} + \gamma \frac{kT}{q} \ln X \qquad \text{(C8)}$$

but with the diode ideality factor γ replaced by the sum of the subcell ideality factors:

$$\sum_{i=1}^{\text{total \# subcells}} \gamma_i \qquad \text{(C9)}$$

in the multijunction case.

REFERENCES

[1] King RR, Law DC, Edmondson KM, Fetzer CM, Kinsey GS, Yoon H, Sherif RA, and Karam NH. 40% efficient metamorphic GaInP / GaInAs / Ge multijunction solar cells. *Appl. Phys. Lett.* 2007; **90**, 183516, doi: 10.1063/1.2734507.

[2] Geisz JF, Friedman DJ, Ward JS, Duda A, Olavarria WJ, Moriarty TE, Kiehl JT, Romero MJ, Norman AG, and Jones KM. 40.8% efficient inverted triple-junction solar cell with two independently metamorphic junctions. *Appl. Phys. Lett.* 2008; **93**, 123505, doi:10.1063/1.2988497.

[3] Dimroth F, Guter W, Schone J, Welser E, Steiner M, Oliva E, Wekkeli A, Siefer G, Philipps SP, Bett AW. Metamorphic GaInP/GaInAs/Ge triple-junction solar cells with > 41 % efficiency. *34th IEEE Photovoltaic Specialists Conference (PVSC), Philadelphia, PA* 2009; 1038, doi: 10.1109/PVSC.2009.5411199.

[4] Guter W, Schone J, Philipps SP, Steiner M, Siefer G, Wekkeli A, Welser E, Oliva E, Bett AW, Dimroth F. Current-matched triple-junction solar cell reaching 41.1% conversion efficiency under concentrated sunlight. *Appl. Phys. Lett.* 2009; **94**, 223504, doi: 10.1063/1.3148341.

[5] King RR, Boca A, Hong W, Liu X-Q, Bhusari D, Larrabee D, Edmondson KM, Law DC, Fetzer CM, Mesropian S, and Karam NH. Band-Gap-Engineered Architectures for High-Efficiency Multijunction Concentrator Solar Cells. *24th European Photovoltaic Solar Energy Conference (EU PVSEC), Hamburg, Germany* 2009; 55, ISBN 3-936338-25-6.

[6] AM1.5 Direct Normal spectrum. Standard Tables for Reference Solar Spectral Irradiances: Direct Normal and Hemispherical on 37° Tilted Surface. ASTM Standard G173-03. ASTM International, West Conshohocken, PA, 2003.

[7] King RR, Fetzer CM, Colter PC, Edmondson KM, Ermer JH, Cotal HL, Yoon H, Stavrides AP, Kinsey G, Krut DD, and Karam NH. High-Efficiency Space and Terrestrial Multijunction Solar Cells Through Bandgap Control in Cell Structures. *29th IEEE Photovoltaic Specialists Conference (PVSC), New Orleans, LA* 2002; 776.

[8] King RR, Law DC, Fetzer CM, Sherif RA, Edmondson KM, Kurtz S, Kinsey GS, Cotal HL, Krut DD, Ermer JH, and Karam NH. Pathways to 40%-Efficient Concentrator Photovoltaics. *20th European Photovoltaic Solar Energy Conference (EU PVSEC), Barcelona, Spain* 2005; 118, ISBN 3-936338-19-1.

[9] Zhao J, Wang A, Green MA, and Ferrazza F. Novel 19.8% efficient ''honeycomb'' textured multicrystalline and 24.4% monocrystalline silicon solar cells. *Appl. Phys. Lett.* 1998; **73**, pp. 1991-1993.

[10] Green MA, Emery K, Hishikawa Y, and Warta W. Solar cell efficiency tables (version 35). *Prog. Photovolt: Res. Appl.* 2010; **18**, 144, doi: 10.1002/pip.974 .

[11] Shockley W and Queisser HJ. Detailed Balance Limit of Efficiency of p-n Junction Solar Cells. *J. Appl. Phys.* 1961; **32**, 510, doi:10.1063/1.1736034.

[12] Marti A, Balenzategui JL, Reyna RF. Photon recycling and Shockley's diode equation. *J. Appl. Phys.* 1997; 82, pp. 4067-4075.

[13] Létay G, Baur C, Bett AW. Theoretical Investigations of III-V Multi-junction Concentrator Cells Under Realistic Spectral Conditions. *19th European Photovoltaic Solar Energy Conf.* 2004; 187-190.

[14] King RR, Sherif RA, Law DC, Yen JT, Haddad M, Fetzer CM, Edmondson KM, Kinsey GS, Yoon H, Joshi M, Mesropian S, Cotal HL, Krut DD, Ermer JH, and Karam NH. New Horizons in III-V Multijunction Terrestrial Concentrator Cell Research. *21st European Photovoltaic Solar Energy Conference (EU PVSEC), Dresden, Germany* 2006; 124, ISBN 3-936338-20-5.

[15] Kinsey GS and Edmondson KM. Spectral Response and Energy Output of Concentrator Multijunction Solar Cells. *Progress in Photovoltaics: Research and Applications* 2009; **17**, 279-288, doi: 10.1002/pip.

[16]   Newman F, Aiken D, Patel P, Chumney D, Aeby I, Hoffman R, and Sharps P. Optimization of inverted metamorphic multijunction solar cells for field-deployed concentrating PV systems. *34th IEEE Photovoltaic Specialists Conference (PVSC)* 2009; 1611-1616, doi: 10.1109/PVSC.2009.5411385 .

[17]   Philipps SP, Peharz G, Hoheisel R, Hornung T, Al-Abbadi NM, Dimroth F and Bett AW. Energy harvesting efficiency of III-V triple-junction concentrator solar cells under realistic spectral conditions. *Solar Energy Materials and Solar Cells* 2010; **94**, 869-877, ISSN 0927-0248, doi: 10.1016/j.solmat.2010.01.010.

[18]   Dimroth F, Philipps SP, Peharz G, Welser E, Kellenbenz R, Roesener T, Klinger V, Oliva E, Steiner M, Meusel M, Guter W, Bett AW. Promises of Advanced Multi-junction Solar Cells for the Use in CPV Systems. *35th IEEE Photovoltaic Specialists Conf. (PVSC), Honolulu, HI* 2010.

[19]   Gueymard CA. SMARTS, A Simple Model of the Atmospheric Radiative Transfer of Sunshine: Algorithms and Performance Assessment. Technical Report No. FSEC-PF-270-95. (Cocoa, FL, Florida Solar Energy Center, 1995).

[20]   Gueymard CA. Parameterized Transmittance Model for Direct Beam and Circumsolar Spectral Irradiance. *Solar Energy* 2001; **71**, 325-346.

[21]   King RR, Law DC, Edmondson KM, Fetzer CM, Sherif RA, Kinsey GS, Krut DD, Cotal HL, and Karam NH. Metamorphic and Lattice-Matched Solar Cells Under Concentration. *4th World Conf. on Photovoltaic Energy Conversion and 32nd IEEE Photovoltaic Specialists Conf. (PVSC)* 2006; 760-763.

[22]   Adachi S. GaAs and Related Materials. (World Scientific, River Edge, New Jersey, 1994), pp. 232-233.

[23]   Hall RN. Recombination processes in semiconductors. *Proceedings of the IEE - Part B: Electronic and Communication Engineering* 1959; **106**, 923, doi: 10.1049/pi-b-2.1959.0171 .

[24]   van Roosbroeck W, Shockley W. Photon-Radiative Recombination of Electrons and Holes in Germanium. *Physical Review* 1954; **94**, 1558.

[25]   Bardeen J, Blatt FJ, Hall LH. Indirect Transitions from the Valence to the Conduction Bands. *Photoconductivity Conference* (John Wiley, 1956), p. 146.

[26]   Kurtz S, Myers D, McMahon WE, Geisz J, and Steiner M. A Comparison of Theoretical Efficiencies of Multijunction Concentrator Solar Cells. *Prog. Photovolt: Res. Appl.* 2008; **16**, pp. 537–546, doi: 10.1002/pip.830.